High-Gain, High Transmissibility PZT Displacement Amplification Using a Rolling-Contact Buckling Mechanism and Preload Compensation Springs

James Torres and H. Harry Asada, *Member, IEEE*

***Abstract*—A novel design concept of piezoelectric actuators producing large displacement while transmitting a significant amount of energy is presented. A rolling-contact buckling mechanism with a novel preload mechanism can amplify the PZT stack's displacement on the order of 100 times while transmitting several times larger work output than conventional flexure-type displacement amplification mechanisms. Existing displacement amplification mechanisms are analyzed in terms of transmissibility and are characterized with two lumped-parameter elements: serial and parallel compliances. The maximum transmissibility is attained when the parallel stiffness and the serial compliance are zero. An existing flexure mechanism using structural buckling, that produces a large displacement but a low transmissibility, is replaced by a rolling-contact mechanism that approaches the maximum criterion. Furthermore, a mechanism is presented to apply a constant preload to each PZT stack despite their movement. A prototype has been built to implement the design concept and verify the theoretical results. Experiments using the prototype demonstrate that it produces a 4.2 mm free displacement with over 60% transmissibility.**

***Index Terms*—Buckling, displacement amplification, kinematics, mechanism design, piezoelectric actuators, smart actuators, transmissibility.**

I. Introduction

CAPACITIVE actuators, such as piezoelectric actuators, consume virtually no energy for generating a force while maintaining a constant position. In contrast, electromagnetic actuators consume energy whenever a torque is generated. The current drawn to the electromagnetic actuator not only consumes a substantial amount of energy, but also generates heat that often must be removed with a bulky heat sink or a forced cooling system. Grounded robots must bear substantial gravity loads and other noninertial loads for a long period of time. Fig. 1 shows experimental data of an elbow's torque and speed when a robot performed a sequence of tasks, which includes holding a hand drill and making a hole on a workpiece [1]. From the data, we find that over 80% of the time the actuator has to bear a nearly constant load at a stationary position. For the rest of the time, it has to move at a given speed, while exerting a certain torque. Although the torque–speed data varies depending

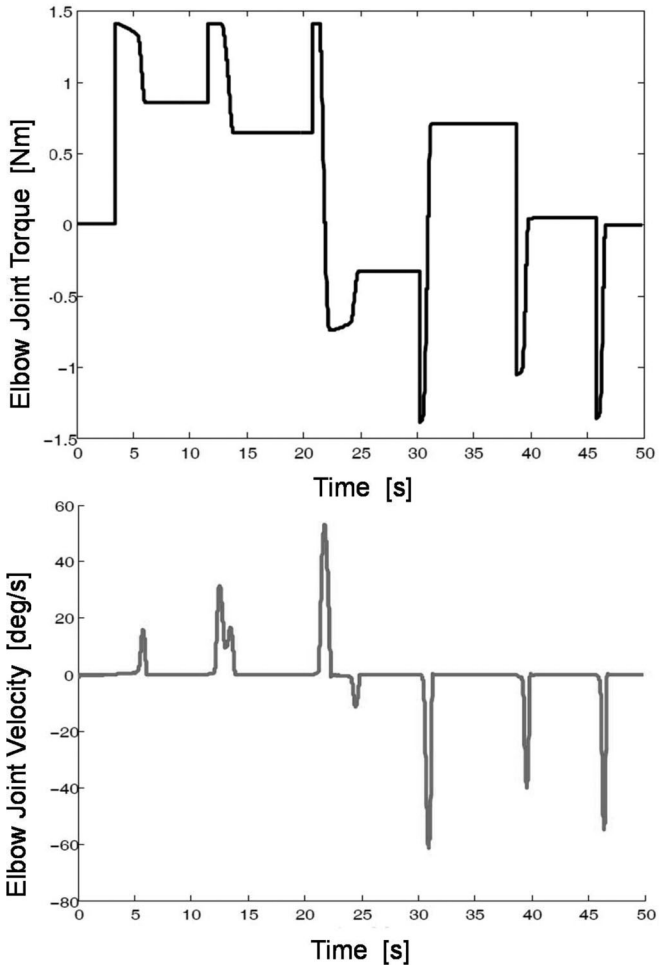

Fig. 1. Experimental data of joint torque and joint speed when a manipulator robot was performing a manufacturing job. Over 80% of the time, the actuator driving the elbow joint was bearing piecewise constant loads.

Manuscript received May 28, 2013; revised December 11, 2013; accepted January 16, 2014. Date of publication February 27, 2014; date of current version August 4, 2014. This work was supported in part by the National Science Foundation under Grant NSF CMMI-1000727, and in part by Sumitomo Heavy Industries, Ltd. This paper was recommended for publication by Editor B. J. Nelson upon evaluation of the reviewers' comments.

J. Torres and H. H. Asada are with the Department of Mechanical Engineering, Massachusetts Institute of Technology, Cambridge, MA 02139 USA (e-mail: jtorres9@mit.edu; asada@mit.edu). This paper has supplementary downloadable material available at http://ieeexplore.ieee.org.

This paper has supplementary downloadable material available at http://ieeexplore.ieee.org, provided by the author. There are two videos. The first video, titled TRO_BucklingActuatorMovie.wmv, shows the rolling-contact buckling actuator, presented in the paper, quasi-statically activated with a 1-Hz sinewave. This results in both monopolar, showed first with a displacement of 1.7 mm, and bipolar, showed second with a peak-to-peak displacement of 3.4 mm, motions. Finally, stills are shown to compare the extremities of the bipolar motion. The second video, titled AssemblyVideoTRO.wmv, is a collection of images detailing the assembly process specifics, including the preload process. Contact jtorres9@mit.edu for further questions about this work.

Color versions of one or more of the figures in this paper are available online at http://ieeexplore.ieee.org.

Digital Object Identifier 10.1109/TRO.2014.2301535

1552-3098 © 2014 IEEE. Personal use is permitted, but republication/redistribution requires IEEE permission.
See http://www.ieee.org/publications_standards/publications/rights/index.html for more information.

on the task, it is noticeable that a significant length of the time is spent maintaining a nearly constant torque with virtually no motion. During these periods of time the robot is not idle; the drilling task is being performed, and a workpiece is being held firmly. Electromagnetic actuators, which dominate today's robotic applications, are clearly not advantageous since they need an electric current to generate these torques. This fact motivated the present work toward PZT actuators. By eliminating energy consumption for bearing nearly constant torque loads, we can significantly improve the actuators' energy efficiency.

On top of the salient potential feature, piezoelectric materials, such as Lead Zirconate Titanate (PZT), have several competitive properties including efficiency and power density, when compared with other smart materials. However, there are a few critical drawbacks that limit the applicability of PZT to broad robotic systems. The most serious drawback is the fact that PZT stacks produce an extremely small strain, on the order of 0.1% [2]. Extracting useful energy from it requires some form of mechanism. Ultrasonic motors, for example, use a friction-drive mechanism to extend tiny cyclic movements into large displacements [3]. Ultrasonic motors are effective in producing precision positioning under limited force applications. Despite successful applications to specific devices and systems, the friction drive mechanism entails tight control of contacting surfaces, which is often difficult. Ultrasonic motors are primarily positioning actuators and are unable to control force, which is a crucial feature in robotic applications [4].

Another type of mechanism used for transmitting the output of the PZT stack to a mechanical load is through externally leveraged displacement amplification mechanisms [4], [5]. Flexures are the most prevailing means to amplify the tiny motion of PZT devices, such as bridge-type mechanisms in macroscale [6] or MEMS scale [7], the "Cymbal" design [8], or in stage motion mechanisms [9]. Beyond flexures, there are several mechanisms that rely on a similar geometric setup including the "X-Frame" [10] and the "V-Stack" [11]. These externally leveraged mechanisms can amplify displacement on the order 10 times. To increase the amplification gain, multistage amplification has been adopted [12], [13]. The nested rhombus mechanism, for example, can produce over 80 times larger displacement in two stages.

One critical issue of those flexure mechanisms is that the net output work transmitted through the flexure is substantially lower than the potential work output that PZT actuators can produce. Due to the compliance at the flexure, the force generated by a PZT stack does not reach its expected value. Also reducing the output work is stiffness at the flexure joints; the output displacement of a PZT stack is significantly lower than its maximum, i.e., free displacement. There is a significant design tradeoff when considering the flexure stiffness. The mechanism must be stiff enough to maintain the force transmitted, but not so stiff such that it restricts the output displacement [6], [8], [11]. Due to these conflicting requirements, the single-stage amplification gain is only on the order of 10, while reducing the possible output energy by a factor of a half. Although the multistage mechanisms can produce a higher amplification gain, the transmitted energy is reduced further. These properties of flexures substantially reduce the energy transmissibility of displacement amplification mechanisms.

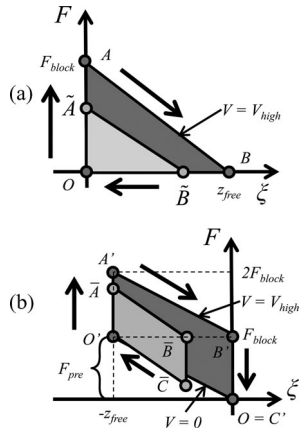

Fig. 2. Cyclic loading and output work of a PZT stack in the force–displacement plane. (a) Maximum work output trajectory for a PZT stack without a preload ABO and that of a PZT stack coupled with a compliant mechanism $\tilde{A}\tilde{B}O$. (b) The maximum work output trajectory for a preloaded PZT stack $A'B'C'O'$ and that of a preloaded PZT coupled with a compliant mechanism $\bar{A}\bar{B}\bar{C}O'$.

The goal of this study is to develop a PZT actuator mechanism that: 1) produces a large displacement amplification gain on the order of 100, and 2) effectively transduces a large output work close to its theoretical limit. In the following, the theoretical limit of a PZT output work and a derivation of the conditions for generating the maximum output energy is addressed. Second, a novel flexure-free displacement amplification mechanism exploiting structural buckling that closely meets the conditions for generating the maximum output energy will be presented. No flexure is used; all components make rolling contacts and the contact forces do not rely on friction. Furthermore, a novel preload technique that applies an approximately constant preload to PZT stacks will be presented in order to double the output work. The new mechanism is implemented and the theoretical results are verified through experiments using a prototype device. An early version of the work has been published in a conference proceeding paper [14]. Complete analysis, including energy transmissibility and preload compensation springs (PCSs), as well as design, implementation, and experimental details of the rolling contact amplification mechanism are presented in the following sections.

II. Theoretical Analysis

Consider a force–displacement plane, as shown in Fig. 2. Suppose that the actuator follows one cycle of a trajectory within this plane. The work produced by the actuator is given by the closed loop integral within the force–displacement plane

$$W_{\text{out}} = \oint F \cdot d\xi. \tag{1}$$

Maximizing this work output we can fully exploit the potential of a PZT stack. For simplicity, assume a linear force–displacement property, as shown in Fig. 2(a). For a given maximum voltage to apply, the maximum work output is determined

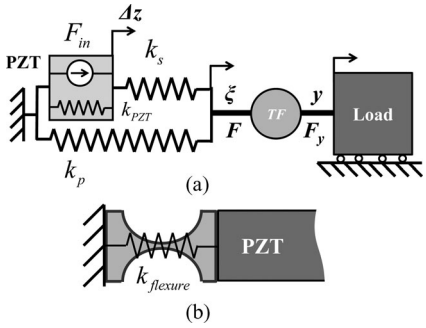

Fig. 3. Schematic of the mechanism compliance in between the PZT stack and the output load, shown as (a) an icon model consisting of a displacement amplification transformer, a parallel spring, a serial spring, and a PZT having its own stiffness and (b) a flexure mechanism as an example of parallel and serial compliance.

by the area of the triangle connecting the origin O, the blocking force, $F_{\rm block}$ at point A, and the free displacement, $z_{\rm free}$ at point B, if the PZT stack can only be loaded under a compressive force $F \geq 0$.

In reality, however, the net usable work output is by far smaller than this theoretical limit. In particular, when a flexure mechanism is used for amplifying the displacement, the flexure reduces the structural stiffness, while impeding the movement of the PZT stack. In general, the static characteristics of such displacement amplification mechanisms can be represented by a simple icon model, as shown in Fig. 3(a). The main functionality of the mechanism is displacement amplification, which is modeled as an ideal transformer TF. The functional relationship between input displacement ξ and output displacement y determines the amplification gain. The displacement ξ, however, is smaller than the one produced by the PZT stack due to the compliance of the amplification mechanism. The compliant elements distributed across the mechanical structure can be lumped in to two springs: one serial spring with stiffness k_s and one parallel spring with stiffness k_p, as shown in Fig. 3(a). The PZT stack itself contains stiffness $k_{\rm PZT}$. For the purposes of this comparison analysis, the hysteresis of the PZT stack is ignored as it is a common factor among all PZT stack actuators [15]. Due to the flexure, the PZT stack has to cope with the additional stiffness k_p that impedes the PZT expansion. Therefore, instead of generating the full free displacement, the displacement at the input port of the transformer ξ, shown in Fig. 3(a), becomes restricted, as shown by point $\tilde{B}$ in Fig. 2(a) [15]. Furthermore, the flexure inevitably exhibits compliance at the joints (narrow slots), as shown in Fig. 3(b), which results in a reduced stiffness in the direction of the output movement. Collectively, these compliance elements can be represented by a serial spring with stiffness k_s between the PZT and the transformer, as shown in Fig. 3(a). Due to this serial compliance, the PZT force transmitted to the transformer cannot reach the highest point, i.e., the blocking force. The PZT force ends up with a lower level, e.g., point $\tilde{A}$ in Fig. 2(a). Overall the work output is reduced, as indicated by the shrunken area of triangle $O\tilde{A}\tilde{B}$ compared with OAB. From this analysis, we can conclude that the ideal displacement amplification mechanism must have an infinitely large serial stiffness and zero parallel stiffness: $k_s \to \infty, k_p = 0$. We can approach these conditions by using a nonflexure type novel design of a buckling displacement amplification mechanism, as described in the following section.

The above maximum work output considers the case where the PZT stack can only be loaded in compression $F \geq 0$. If a negative output force is allowed, the overall work transmitted can be increased. This is achievable with use of a preload mechanism that provides a bias force so that the output force vary in both directions. Suppose that a preload as large as the maximum blocking force is applied. By shifting the origin from point O to point O' in Fig. 2(b), we can redraw the force–displacement plane that is expanded to both directions. The theoretical maximum work output is then doubled compared with before. Note, however, that this analysis is only valid for when the preload is kept constant at a magnitude of at least the blocking force $F_{\rm block}$ despite the PZT stack's displacement. If the preload varies (typically increasing in relation to the output displacement), it can effectively be modeled as an additional parallel stiffness, and hence it would reduce the output work.

The area of the parallelogram $O'A'B'C'$ in Fig. 2(b) is given by $W_{\rm out} = F_{\rm block} \times z_{\rm free}$. Similar to before, this output work can be reduced due to the compliance of the structure. The force is reduced from points A' and C' to points $\bar{A}$ and $\bar{C}$ and the displacement is reduced from point B' to point $\bar{B}$. This reduction in output work can be characterized with a single metric: transmissibility. Transmissibility is defined as the work output of one cycle of actuation normalized by a characteristic energy of the PZT stack $W_{\rm PZT} = F_{\rm block} \times z_{\rm free}$. If k_s' and k_p' are the stiffness of the serial and parallel springs, respectively, normalized by the PZT stiffness, then the transmissibility, η, can be described as the following:

$$\eta \equiv \frac{W_{\rm out}}{W_{\rm PZT}} = \frac{k_s'^2}{(k_s'+1)\left(k_s' + k_p' + k_p' k_s'\right)}. \tag{2}$$

Note that the ideal transformer does not affect the transmissibility, since it is a kinematic component, neither storing nor dissipating energy. Therefore, the above expression gives the transmissibility at the output y. This transmissibility reinforces the previous conclusion that if $k_p = 0$ and $k_s \to \infty$, the transmissibility η approaches 1. The derivation of (2) is shown in Appendix A.

III. Flexure-Free Buckling Displacement Amplification With Preload Compensation

A. Flexure-Free Buckling Mechanism

Our goal is to develop a new amplification mechanism that 1) amplifies displacement on the order of 100 times and 2) achieves a high-energy transmissibility simultaneously. The authors' group has developed a nonlinear displacement amplification scheme utilizing buckling phenomena [16]. Buckling is a prominent nonlinear phenomenon of structure mechanics, which is an unwanted behavior in most applications. However, buckling can produce an order-of-magnitude larger displacement amplification near the singular point. As shown in Fig. 4, a pair of PZT stacks is placed between two rigid walls. The two PZT stacks are

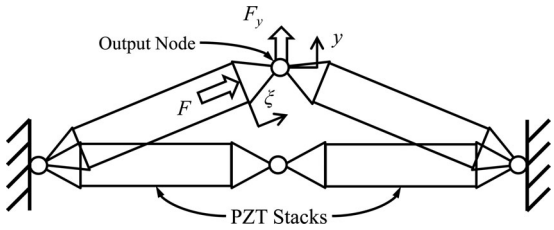

Fig. 4. Kinematic structure of a buckling displacement amplification mechanism, shown both in the kinematic singular configuration, where $\xi = 0$ and $y = 0$, and a displaced condition.

connected in the middle to an element denoted the output node. As a voltage is applied to both PZT stacks, they tend to expand and buckle in one direction perpendicular to their initial alignment. This displacement in the perpendicular direction is typically two orders-of-magnitude larger than the displacement created by the PZT stacks. Furthermore, the buckling mechanism can produce motion on both sides of the singular point, i.e., bipolar motion, with proper mechanisms as detailed in [17], thus doubling the stroke. Our prototype has demonstrated over 100 time larger displacement than that of the PZT stacks. Note that this triple-digit amplification is achieved with a single-stage amplification mechanism.

We propose an innovative flexure-free buckling mechanism that meets all the requirements for achieving the nearly maximum work output as well as large displacement amplification on the order of 100 [14]. To achieve the zero parallel stiffness and the large serial stiffness at the same time, we eliminate the use of flexure from the displacement amplification mechanism. Instead, we have constructed a buckling mechanism satisfying the following conditions.

1) All the components make only rolling contact.
2) They do not slide or slip with respect to each other.
3) The quasi-static contact forces act only in the direction normal to the contacting surfaces.

The last condition above implies that no friction acts at the contact point in statics. Fig. 5 shows the schematic of a mechanism that meets the above conditions. The output node is a center block with two symmetric circular surfaces. Both ends of each PZT stack have a cap with a circular surface of radius r, while the contacting surfaces on the base as well as at the output node are also circular with the same radius R [see Fig. 5(a)]. The characteristic radius Γ is the ratio of the base/output node radius R to the PZT cap radius r. The output node in the middle is constrained such that it can only move linearly in the vertical direction. Suppose that the two PZT stacks are perfectly aligned to the centerline when no voltage is applied [see Fig. 5(a)]. As a high voltage is applied to both PZT stacks at this configuration, they expand simultaneously a distance ξ, causing the mechanism to undergo a buckling phenomenon and the output node displaces a distance y in a vertical direction as depicted in Fig. 5(b). See the supplementary animation video for a demonstration.

Assuming no slip at all the four contacting points, we can find the amplification gain of the ideal transformer. Namely, the ratio of the output displacement to the input displacement ξ can

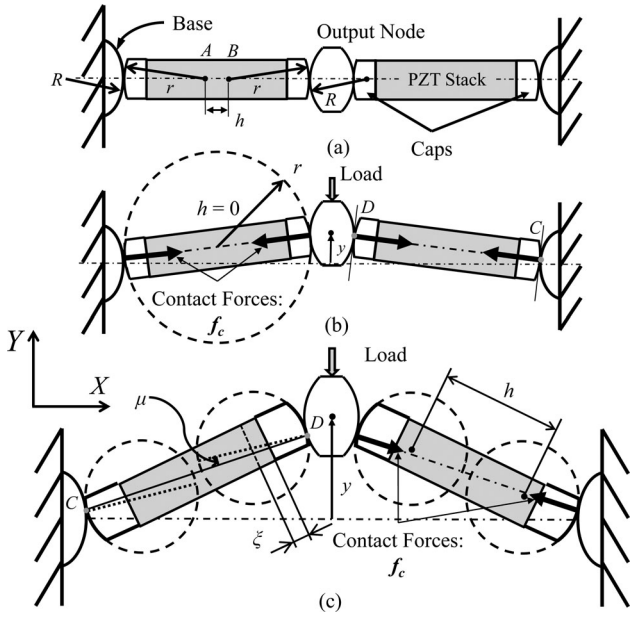

Fig. 5. Schematic of the flexure-free rolling-contact PZT buckling actuator mechanism. (a) In a general case, there is a nonzero distance h between the centers of the caps. (b) If $h = 0$, the frictional component of the contact force becomes negligible. (c) Friction angle μ is related to the distance h and the output displacement y.

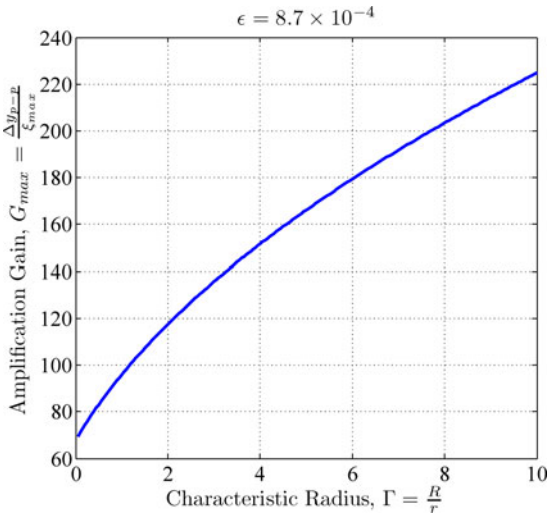

Fig. 6. Plot of the maximum amplification gain $G_{\max} \equiv \frac{\Delta y_{p-p}}{\xi_{\max}}$ as a function of the characteristic radius $\Gamma \equiv \frac{R}{r}$, where Δy_{p-p} is the bipolar peak-to-peak output displacement, $\xi_{\max}$ is the maximum PZT displacement, R is the radius of the base/output node profile, and r is the radius of the caps for an initial cap center distance $h = 0$ and a given radial strain ϵ. The radial strain is defined as $\epsilon \equiv \frac{\xi_{\max}}{r}$.

be approximated to

$$\frac{y}{\xi} \approx \sqrt{\frac{2\left(2(1+\Gamma)r + (1+\Gamma)(h+\xi)\right)^2}{\xi\left(2(1+\Gamma)r + (1+\Gamma)^2 h\right)}}, \quad \xi_{\max} \ll r \qquad (3)$$

where h is the distance between points A and B in Fig. 5(a). See Appendix B for the derivation of (3). We can attain an amplification gain of 100 with practically acceptable values

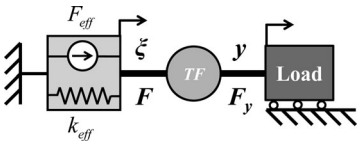

Fig. 7. Reduced model of the PZT stack due to the compliance of the amplification mechanism with an effective force source and PZT stiffness F_{eff} and k_{eff}, respectively. The output of the effective PZT stack is input to the nonlinear transformer that provides the amplification to the overall output load F_y and displacement y.

for R and r (see Fig. 6). A characteristic radius of $\Gamma = 1$, for example, produces an amplification of 96.

As a force acts at the output node in the Y-direction, internal forces are generated at the four contacting points, two of which are labeled as C and D in Fig. 5(b) and (c). An interesting feature of this mechanism is that friction forces vanish at the contacting points if the distance h is zero: $h = 0$. If the distance h is not zero, as illustrated in Fig. 5(c), line $\overline{CD}$ is not aligned with the normal of the contacting surfaces, shown as dotted lines. Since the contact force f_c acts in the direction of $\overline{CD}$, it produces a component in the tangential direction. This means that a static frictional force with magnitude $\sin \mu f_c$ acts at both points C and D. In contrast, if both circular surfaces of each cap are concentric, i.e., $h = 0$, the contacting forces are collinear with line $\overline{CD}$ in Fig. 5(b), and therefore, no tangential component, i.e., no friction force, is induced. Thus, in order for the mechanism to satisfy all of the functional requirements described above, the caps must be concentric, $h = 0$. Note that due to the contact force f_c even a small nonzero displacement h can cause a large frictional force, leading to a significant reduction of the output performance.

Unless disturbed otherwise, the PZT stacks and the output node may not slide relative to each other, because of the absence of forces in the tangential direction. Since all the contacts are rolling contacts, and no force impedes the motion, the parallel stiffness is zero: $k_p = 0$. The circular rolling contact may have a much higher stiffness than that of flexures. In flexure design, there is a tradeoff between the serial and parallel stiffness; a thicker flexure joint yields a stiffer serial spring at a cost of a higher parallel spring stiffness. There is no equivalent conflicting requirement for the rolling contact buckling mechanism. If the parallel stiffness is removed, the transmissibility given by (2) reduces to

$$\eta = \frac{k_s'}{k_s' + 1}, \quad \text{if } k_p' = 0. \tag{4}$$

In general, the model shown in Fig. 3(a) can be reduced to an effective force source and spring in parallel, as shown in Fig. 7. This reduced model is used in the derivation of the amplification mechanism in previous publications [17], [20]. The effective force and stiffness F_{eff} and k_{eff}, respectively, are derived as follows:

$$F_{\text{eff}} = \frac{k_s}{k_s + k_{\text{pzt}}} F_{\text{in}} \tag{5}$$

$$k_{\text{eff}} = \frac{k_s k_{\text{pzt}}}{k_s + k_{\text{pzt}}} + k_p. \tag{6}$$

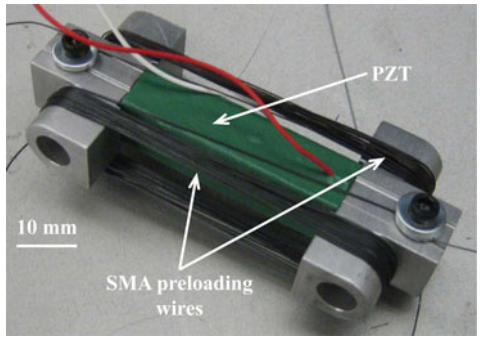

Fig. 8. Preloading a PZT stack using shape memory alloy wires with super-elastic properties.

Note that when $k_p' = 0$, as is the situation described above, $F_{\text{eff}} \to \eta F_{\text{in}}$ and $k_{\text{eff}} \to \eta k_{\text{pzt}}$. Therefore, the transmissibility not only describes the relationship between the actual work output compared with the ideal scenario, but also linearly scales the force output and stiffness when the parallel stiffness vanishes, $k_p = 0$.

B. Preload

The theoretical maximum output work given by $W_{\text{out}} = F_{\text{block}} \times z_{\text{free}}$ is attained when the PZT stack can produce both positive (compressive) and negative (tensile) force. This is achieved with a preload, which can double the theoretical maximum work output provided that the magnitude of the preload is greater than or equal to the blocking force of the PZT stack. Note, however, that this theoretical limit is achieved when the preload is kept constant at a magnitude equal to or higher than the blocking force throughout the displacement of the PZT stack.

Fig. 8 shows a preliminary experiment apparatus for verifying the theoretical limit of work output. A shape-memory alloy (SMA) wire was wound around the PZT stack for preloading the stack. To maintain the constant preload despite the extension of the PZT stack, the stiffness of the wire must be close to zero. Exploiting the super-elasticity of SMA, we have satisfied this constant preload condition. By holding the PZT stack between two rigid structures, the force–displacement trajectory of the preloaded PZT stack has produced nearly the maximum work output.

Preloading the PZT stack utilizing SMA wires is complex and costly. This can be effectively replaced by a simple spring mechanism by exploiting the buckling mechanism. Fig. 9 shows a mechanism for applying a preload. One wall of the buckling mechanism is pushed inward to apply a preload larger than or equal to the blocking force, while holding the voltage at 0 V. As the preload is applied, an instability is caused at the singular configuration, pushing the output node in either vertical direction. As a result, the preload is hardly kept constant as the output node departs the singular position. This problem can be solved effectively by using a simple spring placed at the output node that can apply a constant preload for a broad range of output displacement y. The spring is termed preload compensation springs (PCS).

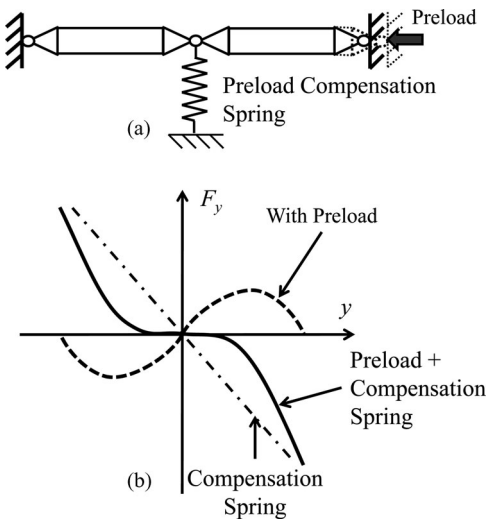

Fig. 9. Benefit of PCSs. (a) Simple schematic of the preload process and corresponding stabilizing spring. (b) Equal magnitude of the initial instability due to preloading and the PCS stiffness.

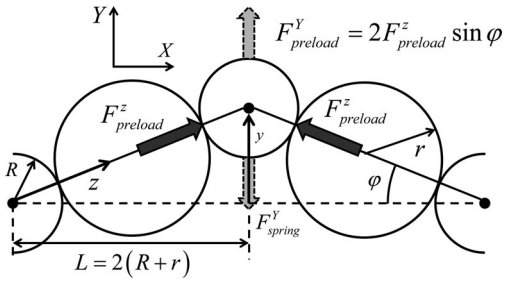

Fig. 10. Schematic detailing the force balance on the output node based on the constant preload force in the direction of the PZT F^z_{preload} and the PCS force $F^Y_{\mathrm{spring}} = k_{\mathrm{PCS}} y$. Note that the preload force in the y-direction F^Y_{preload} is the summation of the two forces in the z-direction. Furthermore, the F^Y_{preload} is exactly balanced by the F^Y_{spring}.

We first consider the necessary condition for the preload force F^z_{preload} to be constant in the direction of z-axis. As shown in Fig. 10, the two preload forces acting from both sides of the PZT stacks create a force in the Y-direction at the output node

$$F^Y_{\mathrm{preload}} = 2F^z_{\mathrm{preload}} \sin\varphi \tag{7}$$

where φ is the angle between the horizontal centerline and the line connecting the two contacting points, as shown in Fig. 10. Assuming that the two circles of the cap surface are concentric, $h = 0$, and that the PZT stack displacement is small, $\frac{\xi}{L} \ll 1$, the direction of the preload force satisfies the following relationship with y:

$$\tan\varphi = \frac{y}{L} \approx \sin\varphi \tag{8}$$

where $L = 2(R + r)$. Substituting (8) into (7), we find that the preload forces in the Y- and z-directions must satisfy the following functional relationship with output displacement y:

$$F^Y_{\mathrm{preload}} = \frac{2F^z_{\mathrm{preload}}}{L} y. \tag{9}$$

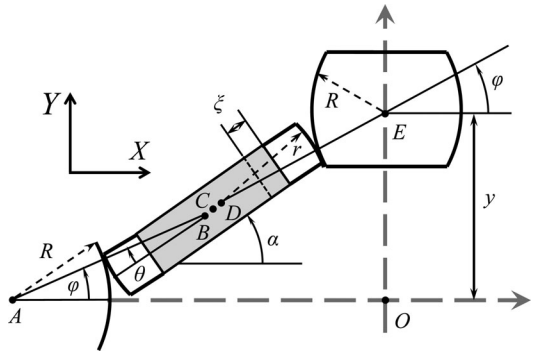

Fig. 11. Labeled schematic of the rolling contact PZT buckling actuator.

Note that the preload force F^z_{preload} must be kept constant, which means that the factors other than the output displacement y in (9) are constant. Replacing the constant factors in (9) with a spring constant

$$k_{\mathrm{PCS}} \equiv \frac{2F^z_{\mathrm{preload}}}{L}. \tag{10}$$

Equation (9) reduces to

$$F^Y_{\mathrm{preload}} = k_{\mathrm{PCS}}\, y. \tag{11}$$

This implies that a spring of stiffness k_{PCS} placed between the output node and the center line can generate a constant preload in the z-direction for an arbitrary output displacement y as long as $\frac{\xi}{L} \ll 1$. At the singular position where the preload has been set, each PZT stack experiences the set preload F^z_{preload}, and the PCS does not affect the PZT stacks since $y = 0$. As the output node deviates from the horizontal centerline, the PCS generates the restoring force $F^Y_{\mathrm{spring}} = k_{\mathrm{PCS}} y$. This balances the force generated by the preload F^z_{preload} in the Y-direction, enabling the PZT stacks to have the constant preload regardless of output displacement y. This is the principle of the PCS.

As long as the PCS has the matched spring constant $k_{\mathrm{PCS}} = \frac{2F^z_{\mathrm{preload}}}{L}$, the singular point at the center becomes a neutrally stable point when the PZT stacks are held at 0 V. This can be explained graphically in Fig. 9(b). The broken line shows the force–displacement characteristics at the output node when the preload alone is applied. Note that the singular point is an unstable equilibrium with the preload alone. In Fig. 9(b), the PCS with the matched spring constant is represented by the straight dash-dot line whose slope has the same magnitude as the unstable slope at the singularity but the opposite sign. Superimposing the two forces generated by the PCS (the straight line) and the preloaded buckling mechanism (the broken line), we find that the singular point is neutrally stable, as shown by the solid curve. Note that the voltage is kept zero in this diagram. As the output node deviates further, the force created by the PCS dominates, creating a large negative force, as shown by the solid curve.

The above argument is based on the approximation of the sine and tangent functions given by (8). As the displacement of the output node extends, this approximation may cause some error. As shown in Fig. 11, the PZT stack's motion is more complex for a large displacement; it rotates as well as expands. The following

analysis using a potential function provides a rigorous argument, and shows that the error of the PCS is negligibly small for a wide range of output node displacement y.

The PCS is connected between point E, shown in Fig. 11, and ground such that the potential energy U_s stored in the spring is equal to $U_s = \frac{1}{2}k_{\rm PCS}y^2$. Also note that the angle of the PZT α is directly related to the displacement angle φ provided the two surfaces do not slip with respect to each other $\alpha = (1+\Gamma)\varphi$. Where Γ, the characteristic radius, is the ratio of the base radius R to the cap radius r: $\Gamma \equiv \frac{R}{r}$. The equivalent force $F^z_{\rm eq}$ is defined as the force from the PCS along the direction of the PZT stack. This force can be determined by differentiating the potential energy U_s with respect to the displacement ξ. Note that due to the complex geometry it is not trivial to put the output displacement y in terms of the displacement ξ. Therefore instead, the displacement angle φ is used as an intermediate variable

$$\xi(\varphi) = L\frac{1-\cos\varphi}{\cos\alpha}$$
$$y(\varphi) = L\sin\varphi + \xi(\varphi)\sin\alpha. \tag{12}$$

By using the chain rule $F^z_{\rm eq}$ is given by

$$F^z_{\rm eq} = -\frac{\partial U_s}{\partial \xi} = -\frac{\partial U_s}{\partial y}\frac{\partial y}{\partial \varphi}\left(\frac{\partial \xi}{\partial \varphi}\right)^{-1}$$
$$\approx -k_{\rm PCS}L\left[1-\left(\Gamma+\frac{1}{2}\right)\Gamma\varphi^2\right]. \tag{13}$$

Over a wide range of characteristic radii, including the characteristic radius used in the implementation described below, the deviation of the preload from its initial value is less than 0.1% over the full range of the buckling amplification mechanism. Considering a preload on the order of the blocking force of the PZT stack, this corresponds to a normalized parallel stiffness, k'_p on the order of 0.001. Therefore, the complex, bulky, and costly SMA wires can be eliminated. The simple spring can approximate the required restoring force accurately. This result is independent of the specific PZT stack properties, provided that the maximum strain is on the order of 0.1%.

IV. Implementation

The design concept of the flexure-free rolling-contact buckling mechanism has been implemented on the prototype test bed shown in Fig. 12. Table I summarizes the major specifications of the prototype. The prototype consists of a pair of PZT stacks encased by end caps in contact with the output node and a pair of base blocks, all of these elements are aligned with the horizontal centerline at rest. A preload adjustment mechanism with load cells is attached at each end. After adjusting the preload, the base blocks are secured with the clamps shown in the figure. There are a few technical issues critical to successful implementation.

1) The output node must be kept upright and aligned with the Y-axis at all times: no rotation, translation, or slip is allowed except for translation in the Y-direction, i.e., the output axis.
2) Tuned PCSs must be attached to the output node.

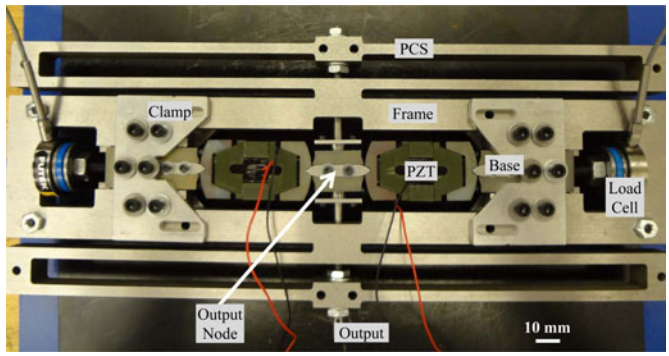

Fig. 12. Test bed of the high-gain rolling-contact PZT buckling actuator.

TABLE I
Tabulated Parameters for the Prototype Shown in Fig. 12

PZT Stack		
Length	36	mm
Free Displacement, z_{free}	52	μm
Blocking Force, F_{block}	4500	N
Stiffness, k_{PZT}	86	$\frac{kN}{mm}$
PZT Constant	30	$\frac{N}{V}$
Maximum Voltage	150	V
Mass, m	0.034	kg
Rolling Contact Amplification Mechanism		
Material	D2 Tool Steel	–
Young's Modulus	210	GPa
Cap Radius, r	25	mm
Cap Crowning Radius	100	mm
Output Node Radius, R	12.5	mm
Output Node Crowning Radius	-120	mm
PCS Stiffness, k_{PCS}	150	$\frac{N}{mm}$
Preload Force, F_{pre}	5600	N
Mass, M	1.86	kg

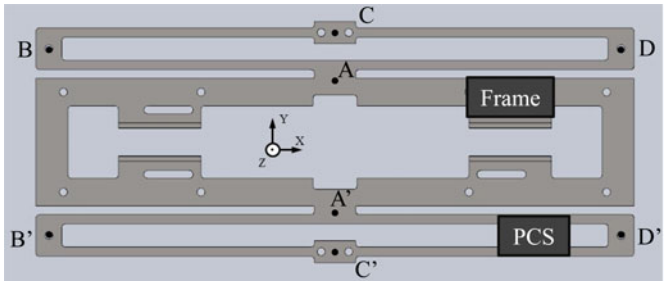

Fig. 13. Solid model of the buckling mechanism frame with PCS integrated into the structure.

3) The structural stiffness that determines the serial stiffness k_s must be substantially higher than that of the PZT stacks.

Fig. 13 shows the frame of the prototype test bed made of steel. Two sets of the slotted beam structure, *ABCD* and $A'B'C'D'$, having a tuned stiffness along the Y-axis, serve as the PCS. As point C is pushed away from point A, the beams are deformed to a rhombus-like shape: the restoring force versus y displacement gives the spring constant. A rod attached to the output node is inserted into a couple of holes at A and A', and is

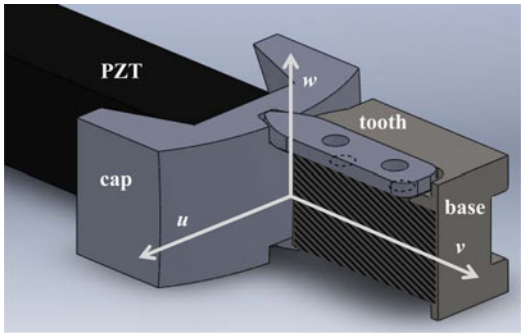

Fig. 14. Labeled diagram of the cap-base profile contact. To avoid friction, there is a designed gap between the gear tooth and the slot on the cap. Ideally, the gear is used only for alignment during assembly and as a failsafe mechanism.

fixed to C and C'. This PCS mechanism plays dual roles. One is to constrain the output node so that it may not rotate about the X-, Y-, and Z- axes as well as restrict translation in the directions perpendicular to the Y-axis. The other is to provide the tuned spring constant so that the middle position ($y = 0$) is neutrally stable, as discussed in the previous section.

To prevent the caps from slipping relative to the output node and base, a slip prevention mechanism has been devised by using a gear tooth meshed with a tight slot. As shown in Fig. 14, any slip in the u-direction between the cap and the ground block may be prevented by a tooth on the ground block inserted into a slot of the cap. Note that the large PZT force does not act on the gear tooth in the v-direction, since the PZT force is borne at the rolling contact area. A small gap between the tooth and the slot relieves the large PZT force. As the cap tends to slip in the u-direction relative to the ground block, the tooth may contact the wall of the slot to prevent further slipping. A pair of the slip prevention mechanisms (i.e., gear teeth) are stationed at both upper and bottom surfaces of each cap and base so that a rotational misalignment about the v-axis in the figure is prevented as well.

The most critical factor that determines the transmissibility is the serial stiffness. According to (4), the serial stiffness must be twice larger than that of the PZT stack in order to attain 60% of transmissibility, and four times larger stiffness for 80% of transmissibility. The most significant cause of compliance is the rolling contact couple shown in Fig. 16. There are four such rolling contacts involved in this displacement amplification mechanism. Fig. 15 plots the stiffness of each rolling contact couple normalized by the PZT stack stiffness computed based on the Hertz contact theory [18] for different contact forces normalized by the PZT stack's blocking force. The solid line is the normalized stiffness when the contacting couple makes a line contact, as illustrated in Fig. 14. Although the highest stiffness is obtained, the line contact between a pair of cylindrical surfaces has two drawbacks. One is that the stiffness significantly reduces as the pair of cylindrical surfaces rotates relative to each other. For example, if the cap in Fig. 14 rotates about the v-axis, the line contact immediately changes to a point contact. This causes a significant reduction of the contact stiffness, as shown by the dotted line in Fig. 15. Another drawback is the stress concentration that may occur near the edges of the contacting

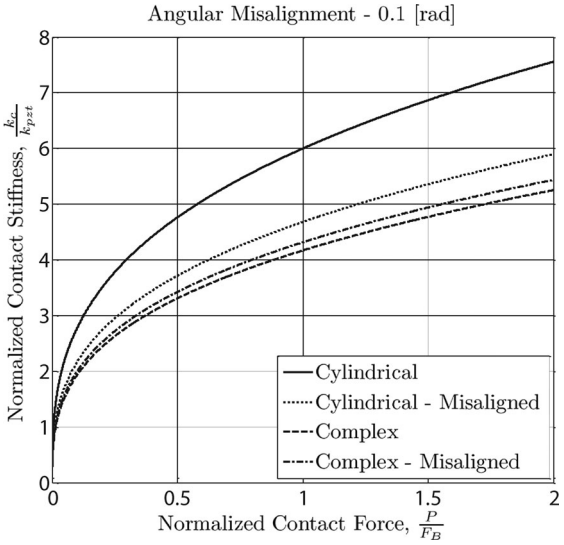

Fig. 15. Plot showing the nonlinear Hertzian contact stiffness for the cylindrical and crowned caps. Note the large deviation in the cylindrical caps due to an angular misalignment of the cap.

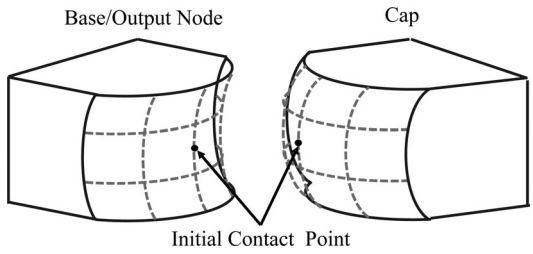

Fig. 16. Simple schematic highlighting the crowning on both the cap and the base profiles. Note the concave crown radius of the base is larger than the convex crown radius of the cap.

line if the two blocks rotate about the u-axis in Fig. 14. To overcome these problems the caps, the base, and the output node are crowned, such that there is an allowable misalignment (see Fig. 16). With crowned surfaces the contact stiffness reduces, as shown in Fig. 15. However, the crowned surfaces have a considerably lower sensitivity to misalignment; less than 5% of reduction is observed for a misalignment of 0.1 radian about the v-axis.

Due to the sensitivity to misalignment and the small displacements associated with the PZT stack, the tolerances of most of the mechanical components within the mechanism are small. Assembly of the mechanism typically requires the ability to adjust several parameters such as the preload displacement/force, the rest length of the PCS and rotation of the PZT stack-cap assembly. These adjustments are shown in greater detail in the attached multimedia.

V. Experimental Results

The prototype PZT actuator with the flexure-free buckling displacement amplification mechanism and the PCSs has been tested experimentally. The modeled serial stiffness is $160\,\frac{\mathrm{kN}}{\mathrm{mm}}$, which is just below twice the PZT stacks stiffness, $k_{\mathrm{PZT}} = 86\,\frac{\mathrm{kN}}{\mathrm{mm}}$. Fig. 17 shows the experiment of output

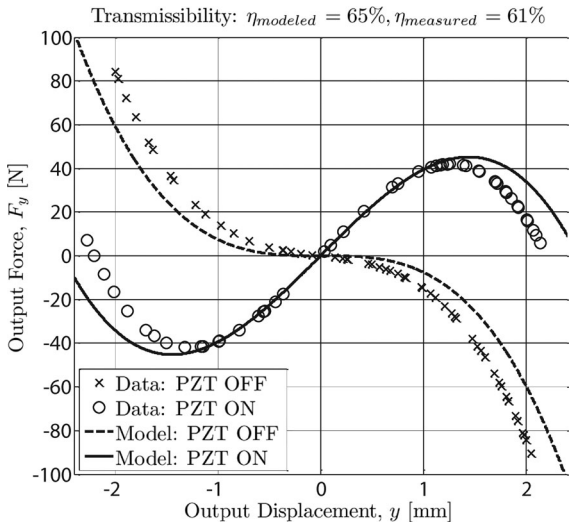

Fig. 17. Plot of the force–displacement trajectory comparing the model of the initial prototype and the measured performance. A measured peak-to-peak displacement Δy_{p-p} of 4.2 mm and transmissibility η of 61% was achieved.

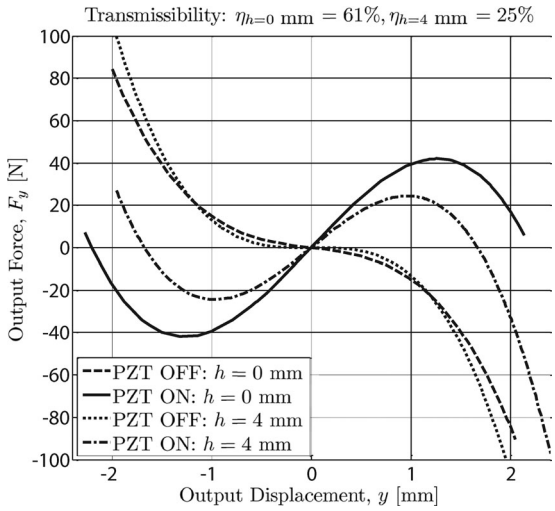

Fig. 18. This plot compares the force–displacement trajectory for the buckling actuator with two separate values of h: $h = 0$ and $h = 4$ mm. When the caps are not concentric, i.e., $h \neq 0$, the combination of the frictional force and the preload limit the overall displacement and greatly limit the output work, hence the reduction in transmissibility from 61% to 25%.

force–displacement characteristics: F_y versus y. A displacement source was aligned in series with a load cell and connected to the output node, allowing for simultaneous measurement of both states. The circles represent the curve when the maximum voltage 150 V was applied, while the crosses are for 0 V. While the maximum voltage is applied, the prototype actuator produced a free displacement of 2.1 mm in either direction with a total net displacement of 4.2 mm due to the bidirectionality and an overall amplification gain of 81. The maximum force was 48 N when the PZT stacks were activated, while a maximum restoring force of 82 N was recorded when the PZT was deactivated, producing 130 N of peak-to-peak maximum force.

A. Discussion

We can evaluate the work output and transmissibility of the prototype PZT buckling actuator based on the output force and displacement data. We can find from the two curves in the force–displacement plane that one cycle of activation and deactivation produces 254 mJ of work output, which corresponds to a transmissibility of 61%. This agrees closely with the analytic estimate of 65%. As analyzed previously, the transmissibility does not depend on the transformer, i.e., the kinematic relationship of displacement amplification. This implies that the work output can be obtained by computing the area covered by one cycle of actuator operation in the output force–displacement plane, i.e., the $F_y - y$ plane. The experimental result of work output 254 mJ was obtained from the area between the two curves in the figure.

The major design parameter that controls the output performance for a given PZT stack and maintaining the constraint $h = 0$ is the characteristic radius Γ. Increasing Γ too much has two major adverse consequences. First, the nonlinear PCS stiffness with respect to the PZT stack displacement will become nonnegligible. Second, with larger rotations, i.e., a larger output displacement, the shear force on PZT stack can become nonnegligible. PZT stack actuators are particularly susceptible to failure via shear forces due to the layered structure. Aside from the characteristic radius, the preload needs to be at least the blocking force, but increasing it further only provides a minimal benefit to the contact stiffness and can cause damage to the PZT stack.

It is important to ensure that the circular surfaces of the caps at both sides of each PZT stack are concentric, $h = 0$. If the concentric condition is violated, frictional forces arise at the rolling contact interfaces, as discussed previously. The frictional force can be significantly large due to the large initial preload, which reduces the net output force and, subsequently, the displacement would reduce. Fig. 18 also shows the experiment of output force–displacement when the two circles are separated by 4 mm, i.e., $h = 4$ mm. Note that both free displacement and maximum force reduced significantly, to the point that the output work reduced to 104 mJ, and the transmissibility reduced to 25%.

VI. Conclusion and Future Work

A new rolling contact buckling mechanism has been presented to take advantage of the capacitive nature of PZT stack actuators. Whereas most displacement amplification designs rely on flexures and a nested architecture to provide large amplification ratios, the rolling contact mechanism was able to create an amplified displacement of two orders of magnitude while maintaining a transmissibility of over 60% within a single stage. This was achieved by

1) increasing serial stiffness and removing parallel stiffness by replacing a flexure joint with a rolling contact joint;
2) removing friction from the contact surfaces by making center of the cylindrical cap profiles concentric, allowing the contact forces to be borne solely by normal components;
3) expanding the work cycle by preloading the PZT stacks;

4) maintaining a constant preload using a PCS that applies a constant preloading force to the longitudinal direction of each PZT stack while causing no increase in parallel stiffness.

Considering future design improvements, the structure of the buckling mechanism can be made much more compact and lightweight. The prototype built was an experimental testbed equipped with many instruments, which are unnecessary. The frame can be made of a lighter material, such as carbon fiber reinforced plastic, that can provide the high stiffness necessary to produce the high transmissibility. Furthermore, the PCS could be significantly reduced in size, provided that the direction of the output displacement can still be sufficiently constrained.

This mechanism can be used directly for applications where a significant holding force must be generated efficiently for long periods of time, while the required stroke of motion is limited. These include valves, clutches, and brakes [19]. Replacing traditional solenoids and electromagnetic actuators with the PZT buckling actuators will significantly reduce energy consumption and heat generation. Furthermore, the PZT buckling actuators can be used for applications needing a long stroke of motion, or infinite rotation, with an additional mechanism. The authors' group is currently developing a long-stroke linear actuator consisting of a half dozen of PZT buckling actuators engaged with a gear rod. The large displacement on the order of a few millimeters created by each PZT buckling actuator allows for pushing the gear teeth and transmitting a force directly to the rod [20]. Compared with traditional ultrasonic motors, which relies on the frictional torque transmission, the rolling contact PZT buckling actuator can directly apply the force to the direction of the load, yielding reliable actuation appropriate for heavy-duty applications.

Appendix A
Derivation of the Mechanism Transmissibility

In order to derive the work output by the PZT stack within an amplification mechanism, the trajectory must be determined using several parameters: the stiffness, free displacement, and blocking force of the PZT stack, k_{PZT}, z_{free}, and F_{block}, respectively, and the serial and parallel stiffness associated with the mechanism k_s and k_p, respectively. The trajectory, shown in Fig. 19, can then be integrated to find the overall work output via (1). Given the points shown in Fig. 19, the total work output is

$$W_{\mathrm{out}} = \frac{F_{\mathrm{block}} z_{\mathrm{free}} k_s^2 k_{\mathrm{PZT}}}{(k_{\mathrm{PZT}} + k_s)(k_{\mathrm{PZT}} k_s + k_{\mathrm{PZT}} k_p + k_p k_s)}. \quad (14)$$

Recognizing that the ideal work output of the PZT stack is $W_{\mathrm{PZT}} = F_{\mathrm{block}} \times z_{\mathrm{free}}$, and the definition of transmissibility is $\eta \equiv \frac{W_{\mathrm{out}}}{W_{\mathrm{PZT}}}$, the transmissibility can be expressed as

$$\eta = \frac{k_s^2 k_{\mathrm{PZT}}}{(k_{\mathrm{PZT}} + k_s)(k_{\mathrm{PZT}} k_s + k_{\mathrm{PZT}} k_p + k_p k_s)}. \quad (15)$$

By substituting $k_s = k_s' \times k_{\mathrm{PZT}}$ and $k_p = k_p' \times k_{\mathrm{PZT}}$ into (15), it becomes (2).

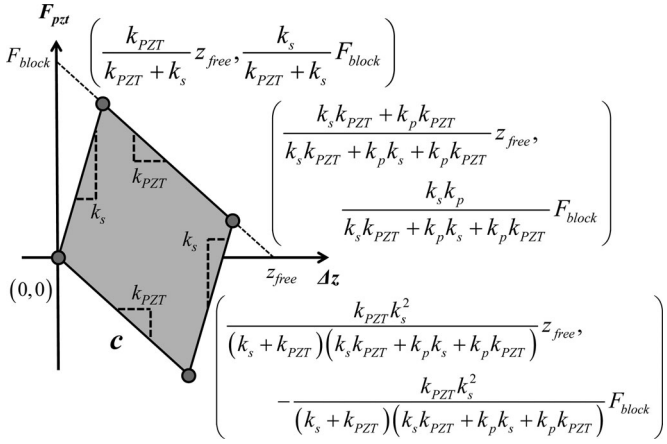

Fig. 19. Force–displacement trajectory c of a PZT stack with stiffness, blocking force, and free displacement of k_{PZT}, F_{block}, and z_{free}, respectively, within a mechanism with a serial and parallel stiffness, k_s and k_p, respectively.

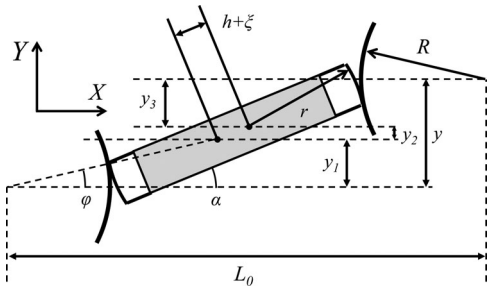

Fig. 20. Schematic of the rolling contact buckling amplification mechanism highlighting the components of the output displacement.

Appendix B
Derivation of the Amplification Gain

The overall output displacement can be broken down into three separate sections, highlighted in Fig. 20. Two symmetric sections associated with the cylindrical profiles rolling along one another, y_1 and y_3, and a middle section associated with the rotation of the PZT stack y_2. Therefore, the displacement of the output can be described as

$$y = y_1 + y_2 + y_3 \quad (16)$$

$$y_1 = y_3 = (R + r)\sin\varphi \quad (17)$$

$$y_2 = (h + \xi)\sin\alpha. \quad (18)$$

There are two constraints associated with the problem. First, it is assumed that there is a no slip rolling condition at the contact points, which yields $\alpha = (1 + \Gamma)\varphi$. The second constraint is that the output node does not translate in the horizontal direction and therefore the horizontal distance is constant throughout the motion of the output, which leads to the following equation:

$$\begin{aligned} L_0 &= 2(R + r) + h \\ &= 2(R + r)\cos\varphi + (h + \xi)\cos\alpha. \end{aligned} \quad (19)$$

Using a second-order approximation for the trigonometric functions, i.e., $\sin\varphi \approx \varphi$ and $\cos\varphi \approx 1 - \frac{1}{2}\varphi^2$, the overall

displacement y can be expressed solely in terms of the geometric constants, R, r, and h, and the extension of the PZT stack ξ. In order to simplify the equation further, it is assumed that $\xi \ll R, r$

$$\varphi = \sqrt{\frac{2\xi}{2(R+r)+(1+\Gamma)^2(h+\xi)}} \tag{20}$$

$$y \approx \left(2(R+r)+(1+\Gamma)(h+\xi)\right)\varphi \tag{21}$$

$$= \sqrt{\frac{\left(2(R+r)+(1+\Gamma)h\right)^2 2\xi}{2(R+r)+(1+\Gamma)^2(h+\xi)}}. \tag{22}$$

Recognizing that $(\Gamma+1)r = R+r$, it is trivial to show that (3) is the same as (22).

REFERENCES

[1] B. Llorens-Bonilla, F. Parietti, and H. Asada, "Demonstration-based control of supernumerary robotic limbs," presented at IEEE/RSJ Int. Conf. Intell. Robots Syst., Vilamoura, Portugal, Oct. 2012, pp. 3936–3942.

[2] J. Huber, N. Fleck, and F. Ashby, "The selection of mechanical actuators based on performance indicies," *Math., Phys. Eng. Sci.*, vol. 453, no. 1965, pp. 2185–2205, 1997.

[3] T. Morita, R. Yoshida, Y. Okamoto, M. K. Kurosawa, and T. Higuchi, "A smooth impact rotation motor using a multi-layered torsional piezoelectric actuator," *IEEE Trans. Ultrason. Ferroelectr. Freq. Control*, vol. 46, no. 6, pp. 1439–1445, Nov. 1999.

[4] C. Niezrecki, D. Brei, S. Balakrishnan, and A. Moskalik, "Piezoelectric actuation: State of the art," *Shock Vibration Digest*, vol. 33, no. 4, pp. 269–280, 2001.

[5] J. Pons, "Piezoelectric Actuators," in *Emerging Actuator Technologies: A Micromechatronic Approach*. Hoboken, NJ, USA: Wiley, 2005, pp. 46–100.

[6] H. Ma, S. Yao, L. Wang, and Z. Zhong, "Analysis of the displacement amplification ratio of bridge-type flexure hinge," *Sens. Actuators A, Phys.*, vol. 132, no. 2, pp. 730–736, 2006.

[7] J. Juuti, K. Kordas, R. Lonnakko, V.-P. Moilanen, and S. Leppavouri, "Mechanically amplified large displacement piezoelectric actuators," *Sens. Actuators A, Phys.*, vol. 120, no. 1, pp. 225–231, 2005.

[8] A. Dogan, K. Uchino, and R. Newnham, "Composite piezoelectric transducer with truncated conical endcaps "Cymbal"," *IEEE Trans. Ultrason. Ferroelectr. Freq. Control*, vol. 44, no. 3, pp. 597–605, May 1997.

[9] K. Choi, J. Lee, and S. Hata, "A piezo-driven compliant stage with double mechanical amplification mechanisms arranged in parallel," *Sens. Actuators A, Phys.*, vol. 161, no. 1, pp. 173–181, 2010.

[10] S. Hall, T. Tzianetopoulou, F. Straub, and H. Ngo, "Design and Testing of a Double X-Frame Piezoelctric Actuator," in *Proc. SPIE Int. Conf. Smart Mater. Struct.*, Mar. 2000, pp. 26–37.

[11] E. Ardelean, D. Cole, and R. Clark, "High Performance 'V-Stack' Piezoelectric Actuator," *J. Intell. Mater. Syst. Struct.*, vol. 15, no. 11, pp. 879–889, 2004.

[12] T. W. Secord and H. Asada, "A variable stiffness PZT actuator having tunable resonant frequencies," *IEEE Trans. Robot. Autom.*, vol. 26, no. 6, pp. 993–1005, Dec. 2010.

[13] J. Ueda, T. W. Secord, and H. Asada, "Large effective-strain piezoelectric actuators using nested cellular architecture with exponential strain amplification mechanisms," *Trans. Mechatronics*, vol. 15, no. 5, pp. 770–782, 2010.

[14] J. Torres, S. Tsukahara, and H. Asada, "Maximizing output work of PZT stacks while gaining large displacement amplification," in *Proc. IEEE Int. Conf. Robot. Autom.*, Karlsruhe, Germany, May 2013, pp. 343–348.

[15] A. Borboni, "Modeling Actuators," in *Meso- to Micro-Actuators: A Theoretical and Practical Approach*. Boca Raton, FL, USA: CRC, 2008, pp. 176–205.

[16] D. Neal and H. Asada, "Nonlinear, large-strain PZT actuators using controlled structural buckling," in *Proc. IEEE Int. Conf. Robot. Autom.*, Kobe, Japan, May 2009, pp. 170–175.

[17] D. Neal and H. Asada, "Bipolar piezoelectric buckling actuators," *IEEE/ASME Trans. Mechatron.*, vol. 19, no. 1, pp. 9–19, Feb. 2014.

[18] W. C. Young, *Roark's Forumlas for Stress and Strain, 6th Ed.* New York, NY, USA: McGraw-Hill, 1989, p. 651.

[19] S. Tsukahara, J. Torres, D. Neal, and H. Asada, "Design method for buckling magnified piezoelectric actuator using flexure joint and its application to a brake system," in *Proc. ASME Dyn. Syst. Controls Conf.*, Ft. Lauderdale, FL, USA, Oct. 2012, pp. 95–102.

[20] J. Torres and H. Asada, "Dynamic analysis of a buckling-type amplification mechanism tomaximize the power output by varying the load impedance and control timing," in *Proc. ASME Dyn. Syst. Controls Conf.*, Ft. Lauderdale, FL, USA, Oct. 2012, pp. 123–130.

James Torres received the B.S. and M.S. degrees in mechanical engineering in 2010 and 2012, respectively, from the Massachusetts Institute of Technology, Cambridge, MA, USA, where he is currently working toward the Ph.D. degree with the Department of Mechanical Engineering.

His current research interests include distributed actuator systems using smart materials, mechatronics, and robotics.

H. Harry Asada (M'89) received the B.S., M.S., and Ph.D. degrees in precision engineering in 1973, 1975, and 1979, respectively, all from Kyoto University, Kyoto, Japan.

He is currently the Ford Professor of mechanical engineering and the Director with the Brit and Alex dArbeloff Laboratory for Information Systems and Technology, Department of Mechanical Engineering, Massachusetts Institute of Technology (MIT), Cambridge, MA, USA. His current robotics research interests includes wearable robots, cellular PZT actuators, and robot applications to aircraft manufacturing and nuclear power plant monitoring. His research in the bioarea focuses on biointegrated robots, where live cells and tissues are used as components. He specializes in robotics, biological engineering, and system dynamics and control.

Dr. Asada received Best Paper Awards at the IEEE International Conference on Robotics and Automation in 1993, 1997, 1999, and 2010; the O. Hugo Schuck Best Paper Award from the American Control Council in 1985; Best Journal Paper Awards from the Society of Instrument and Control Engineers in 1979, 1984, and 1990; and the Best Journal Paper Award from the *Journal of Advanced Robotics* in 2002. He also received the Henry Paynter Outstanding Researcher Award from ASME Dynamic Systems and Control in 1998. More recently, he received the 2011 Rufus Oldenburger Medal from ASME and the Ruth and Joel Spira Award for Distinguished Teaching from the School of Engineering, MIT. He is a Fellow of ASME.